eLIFE
elifesciences.org

Figures and figure supplements

Neuronal connectome of a sensory-motor circuit for visual navigation

Nadine Randel, et al.

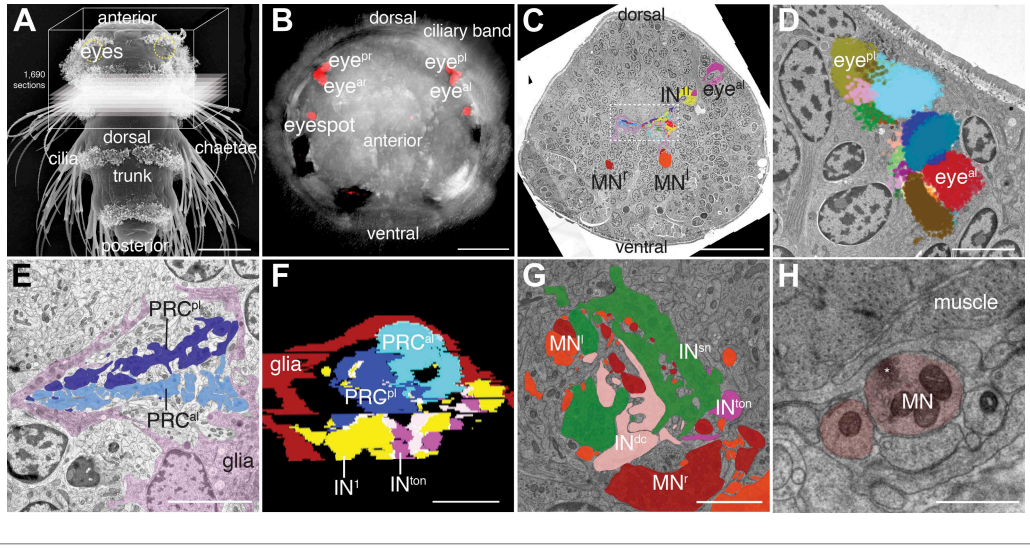

Figure 1. Serial-section electron microscopy imaging of the visual eye circuit in a *Platynereis* larva. (**A**) Scanning electron micrograph of a 72 hr-post-fertilization larva, dorsal view. The boxed volume was sectioned and imaged. (**B**) Anterior view of a 72 hr-post-fertilization larva visualized with differential interference contrast (DIC) optics (grey) showing the position of the eyes visualized by the reflection of the pigments (red). (**C**) A representative electron micrograph from the series with traced neurons. The boxed area contains the primary optic neuropil. (**D**) Reconstruction of the pigment cup of the left anterior and posterior eyes. Pigment granules from the different pigment cells and photoreceptors are colored differently. (**E**) TEM image of the left primary optic neuropil surrounded by glia (pink), with the photoreceptor projections from the anterior and posterior eye colored differently. (**F**) A virtual cross-section of the primary optic neuropil based on ssTEM shows the anterior-posterior layering of glia, photoreceptor, primary interneuron (IN^{1}) and trans-optic-neuropil interneuron (IN^{ton}) processes, anterior is up. (**G**) TEM image of the secondary optic neuropil, with segmented IN^{ton}, IN^{sn} , IN^{dc} and ipsi- and contralateral motorneuron projections. (**H**) TEM image of a neuromuscular synapse from a motorneuron to the ventral longitudinal muscle. Asterisk marks a cluster of synaptic vesicles. Eye^{al}, anterior-left eye; eye^{ar}, anterior-right eye; eye^{pl}, posterior-left eye; eye^{pr}, posterior-right eye; PRC, photoreceptor; IN, interneuron; MN, motorneuron. Scale bars, 50 μm (**A**), 30 μm (**B** and **C**), 5 μm (**D**, **E**, **G**), 1 μm (**F**), 0.5 μm (**H**).

DOI: 10.7554/eLife.02730.003

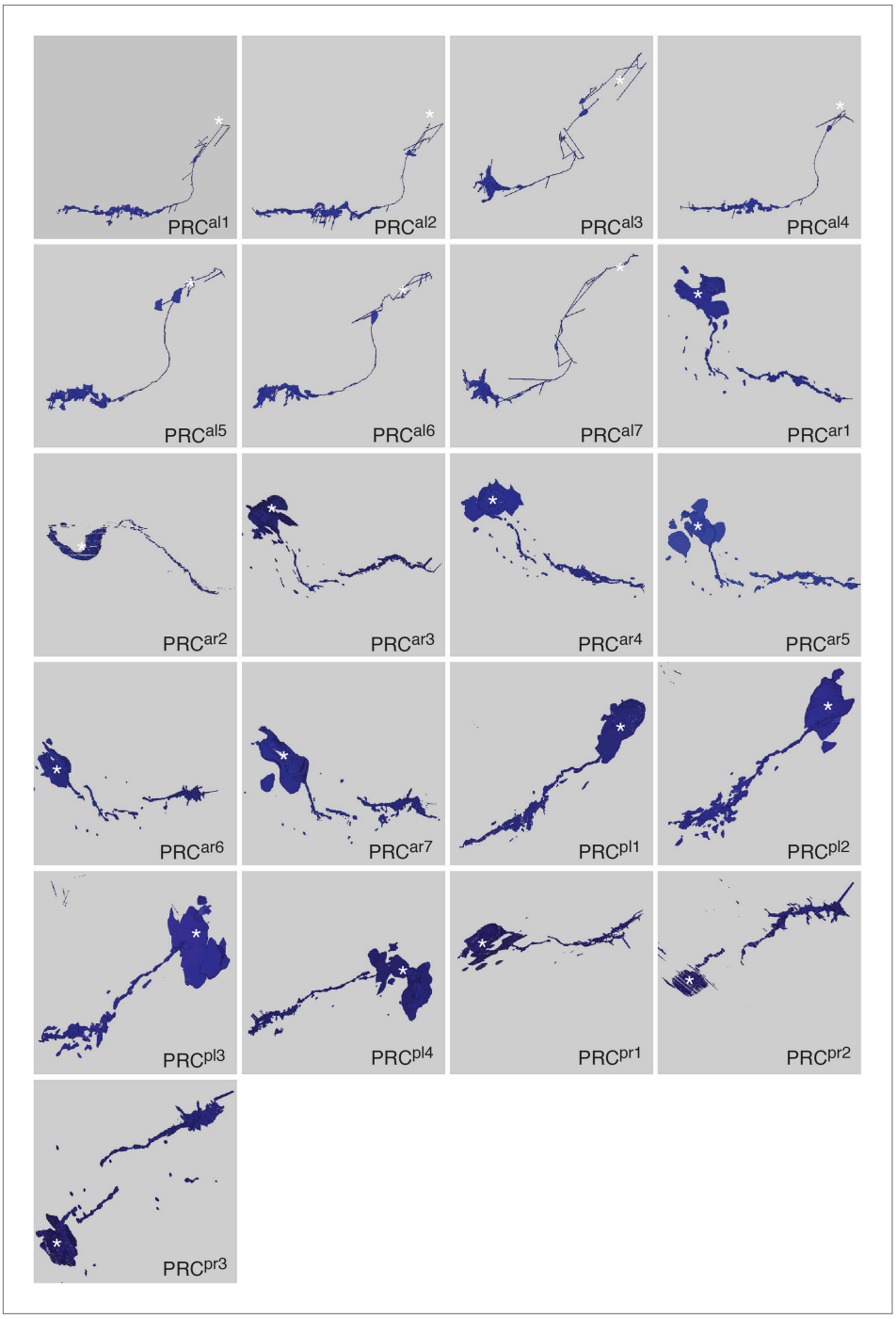

Figure 1—figure supplement 1. Morphology of photoreceptor cells reconstructed from serial TEM sections.

DOI: 10.7554/eLife.02730.004

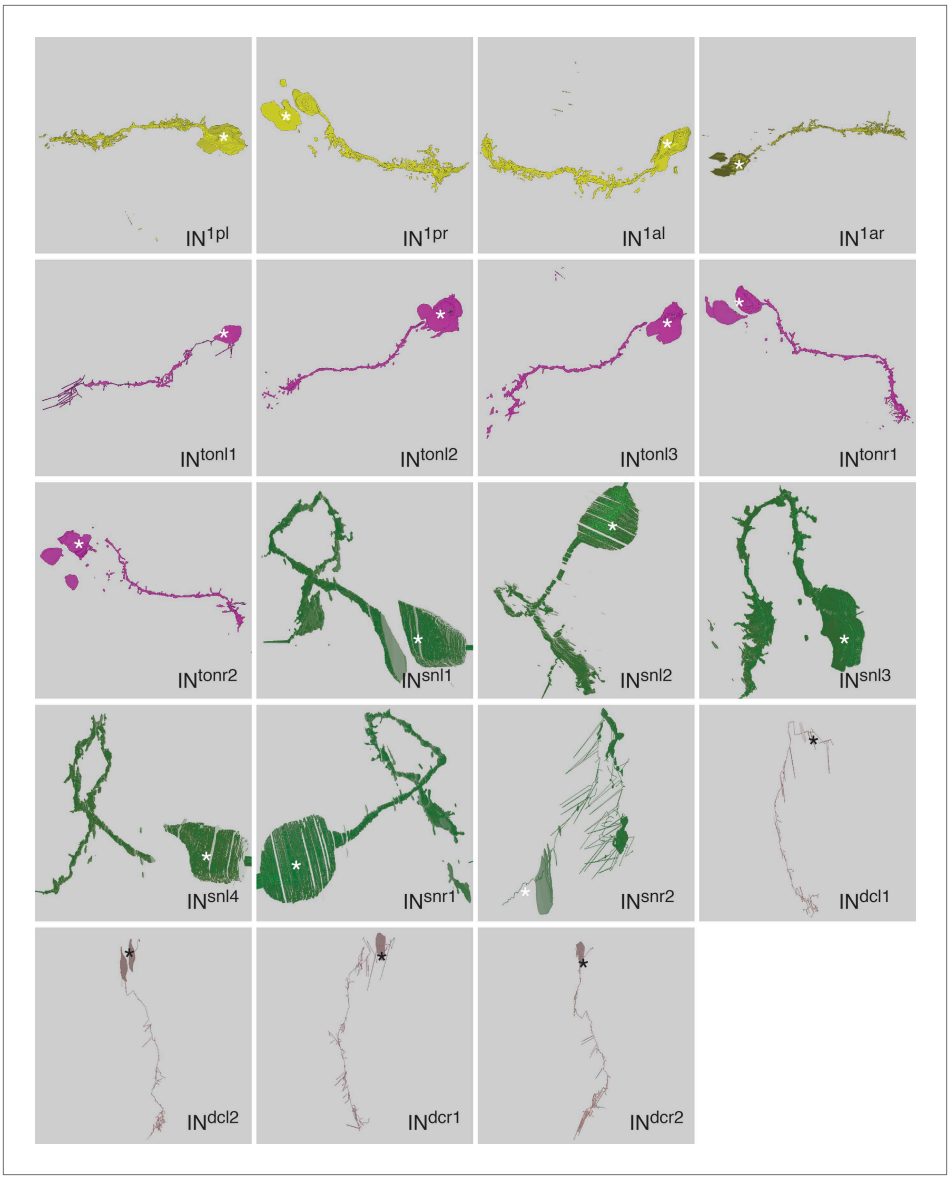

Figure 1—figure supplement 2. Morphology of IN1, IN^{ton}, IN^{sn}, and IN^{dc} cells reconstructed from serial TEM sections.

DOI: 10.7554/eLife.02730.005

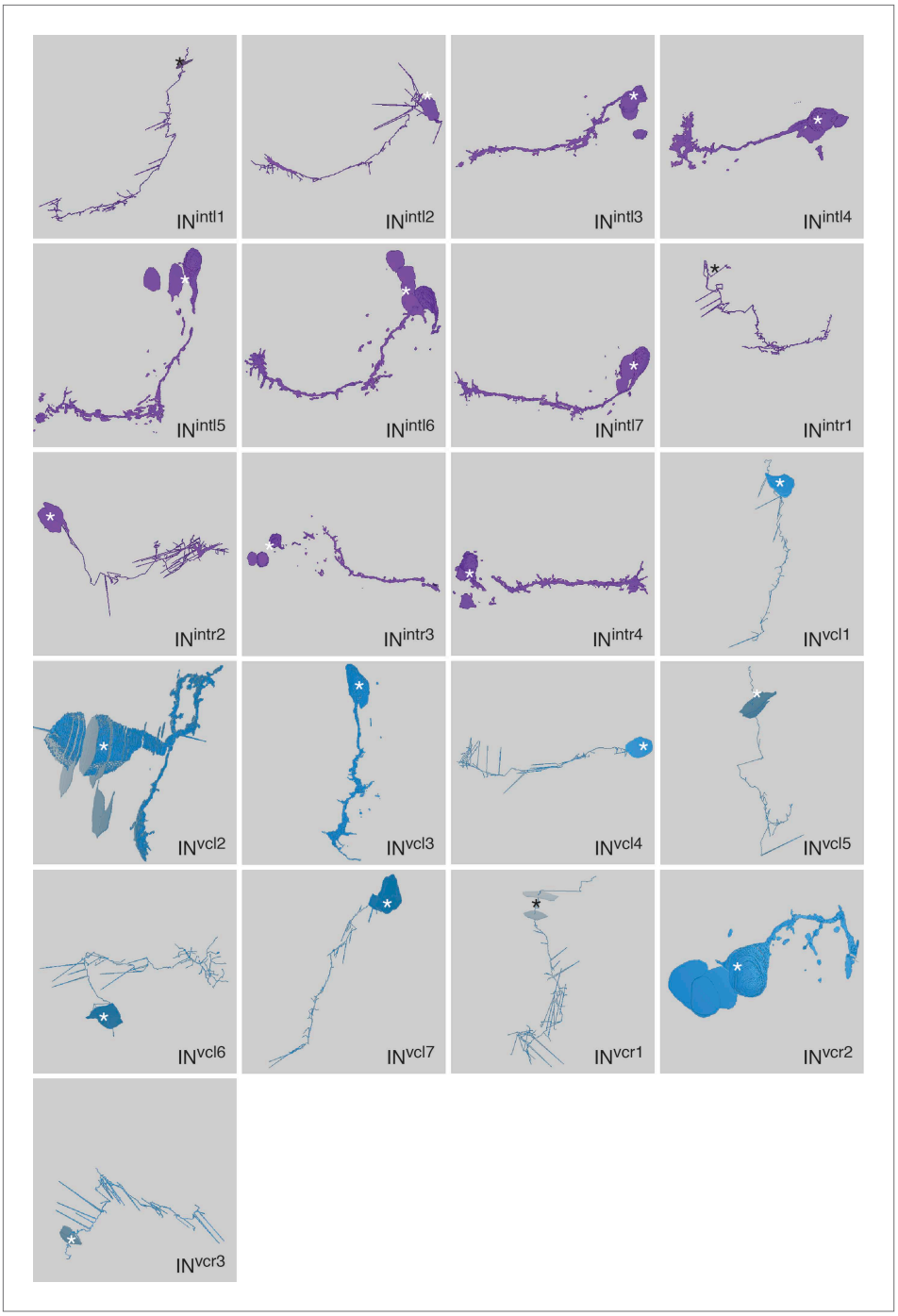

Figure 1—figure supplement 3. Morphology of IN^{int} and IN^{vc} cells reconstructed from serial TEM sections.
DOI: 10.7554/eLife.02730.006

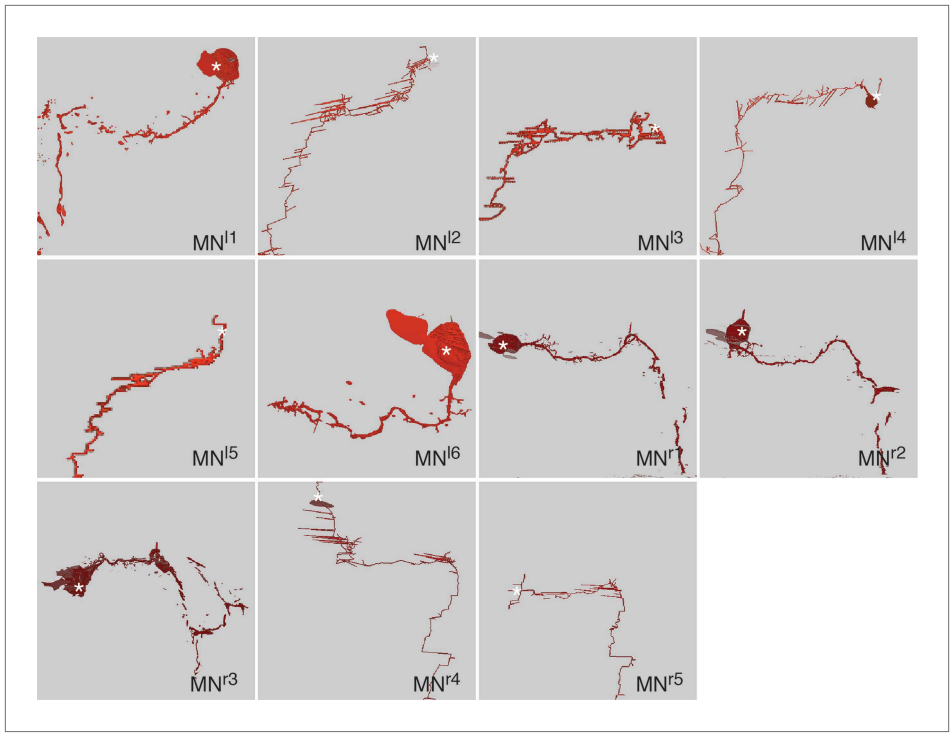

Figure 1—figure supplement 4. Morphology of motorneurons reconstructed from serial TEM sections.
DOI: 10.7554/eLife.02730.007

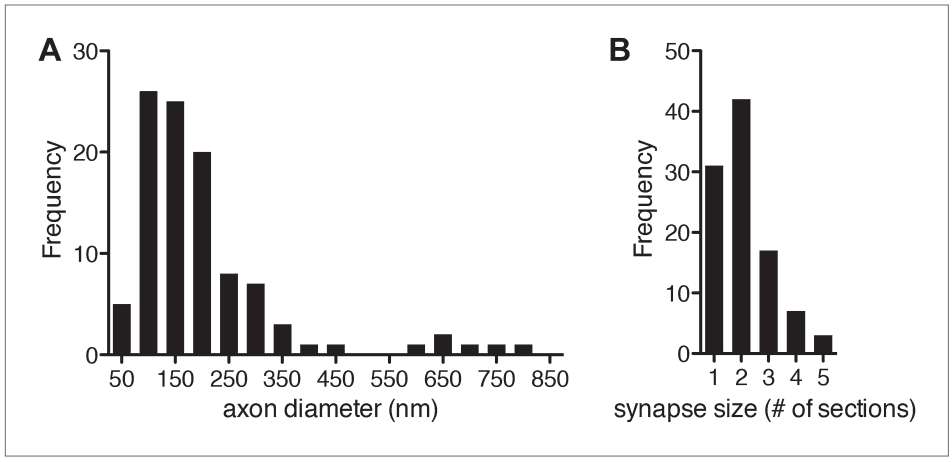

Figure 1—figure supplement 5. Axon diameter and synapse size in the *Platynereis* larval connectome.
DOI: 10.7554/eLife.02730.008

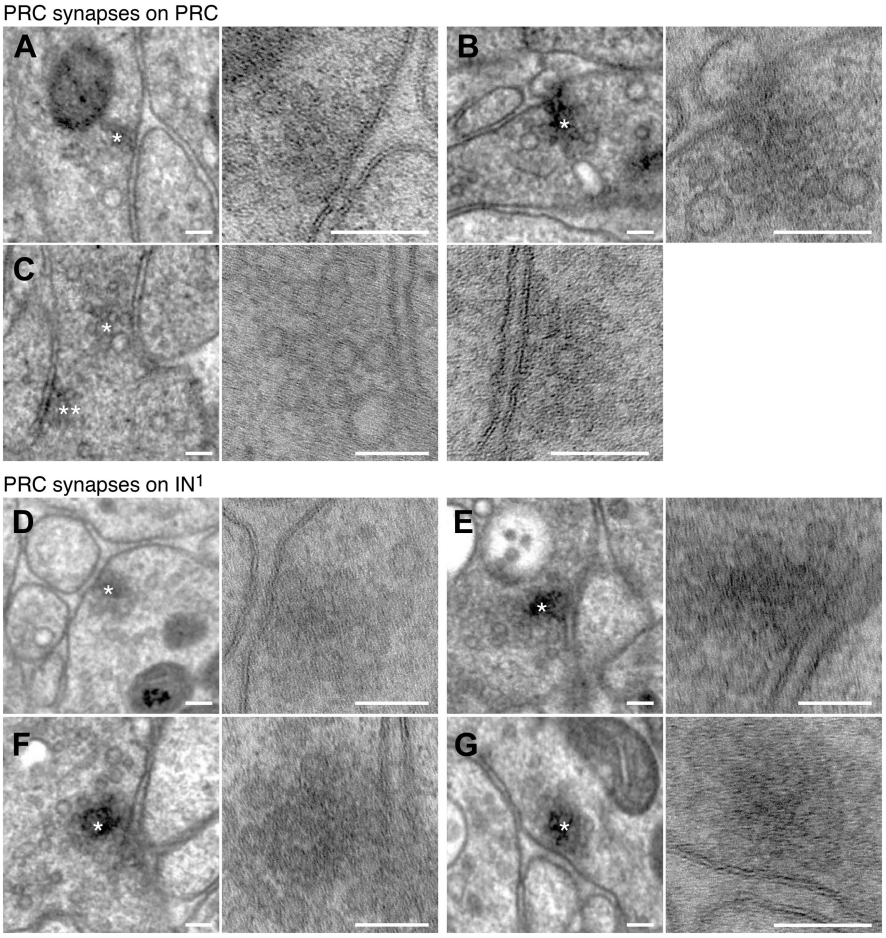

Figure 1—figure supplement 6. Synapses of photoreceptors and IN[1] cells.

DOI: 10.7554/eLife.02730.009

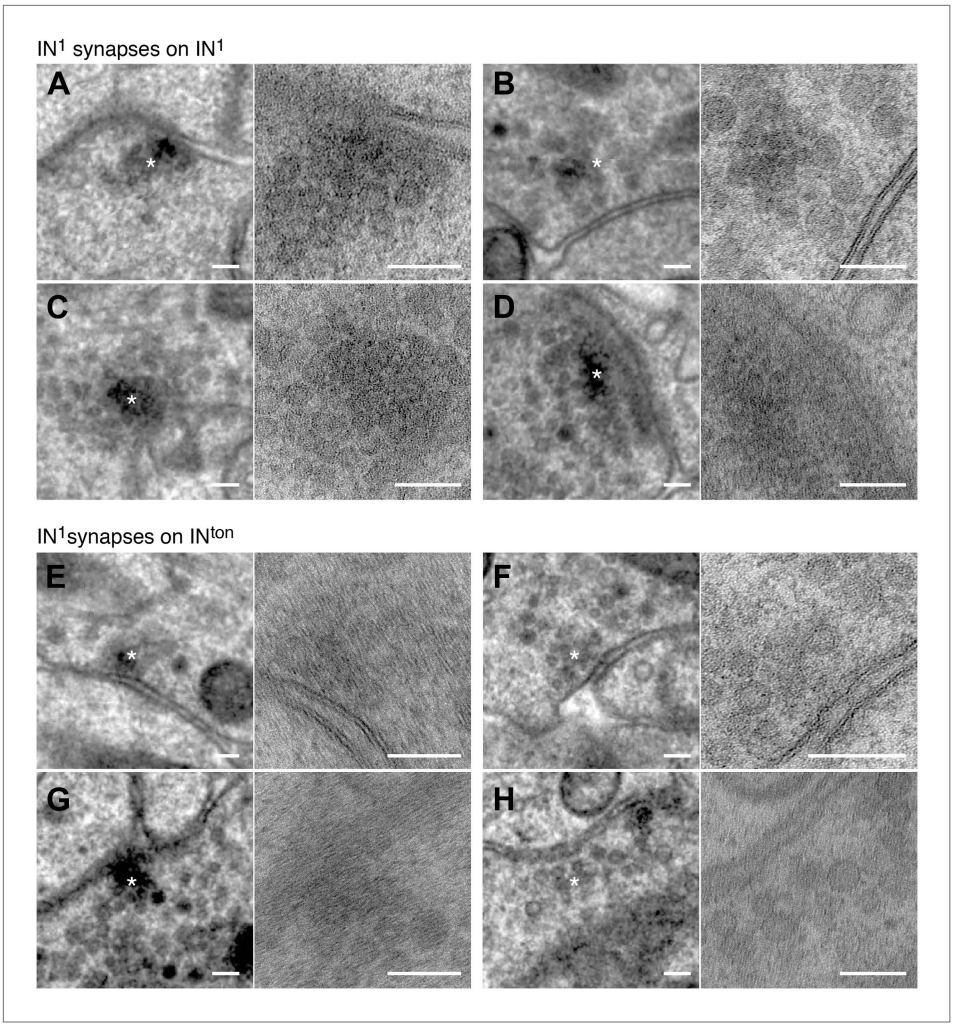

Figure 1—figure supplement 7. Synapses of IN[1] cells.

DOI: 10.7554/eLife.02730.010

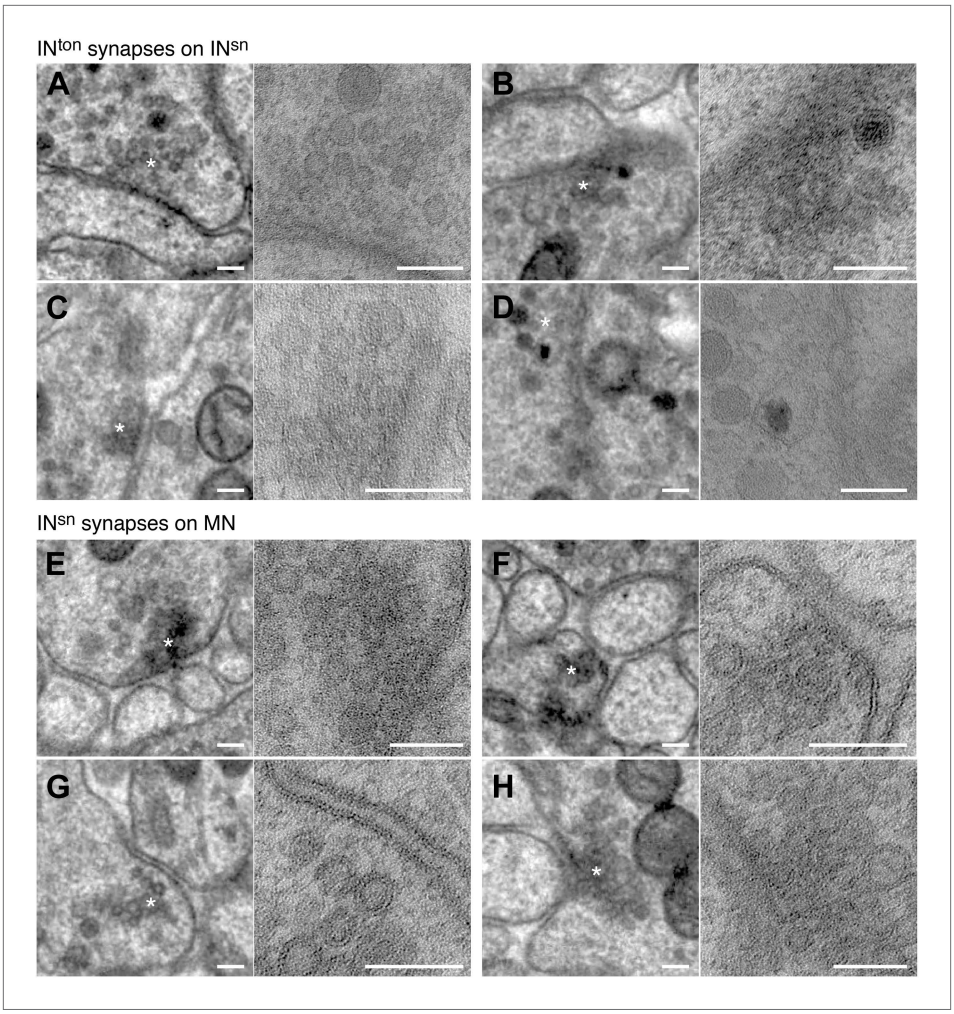

Figure 1—figure supplement 8. Synapses of IN^{ton} cells and IN^{sn} cells.

DOI: 10.7554/eLife.02730.011

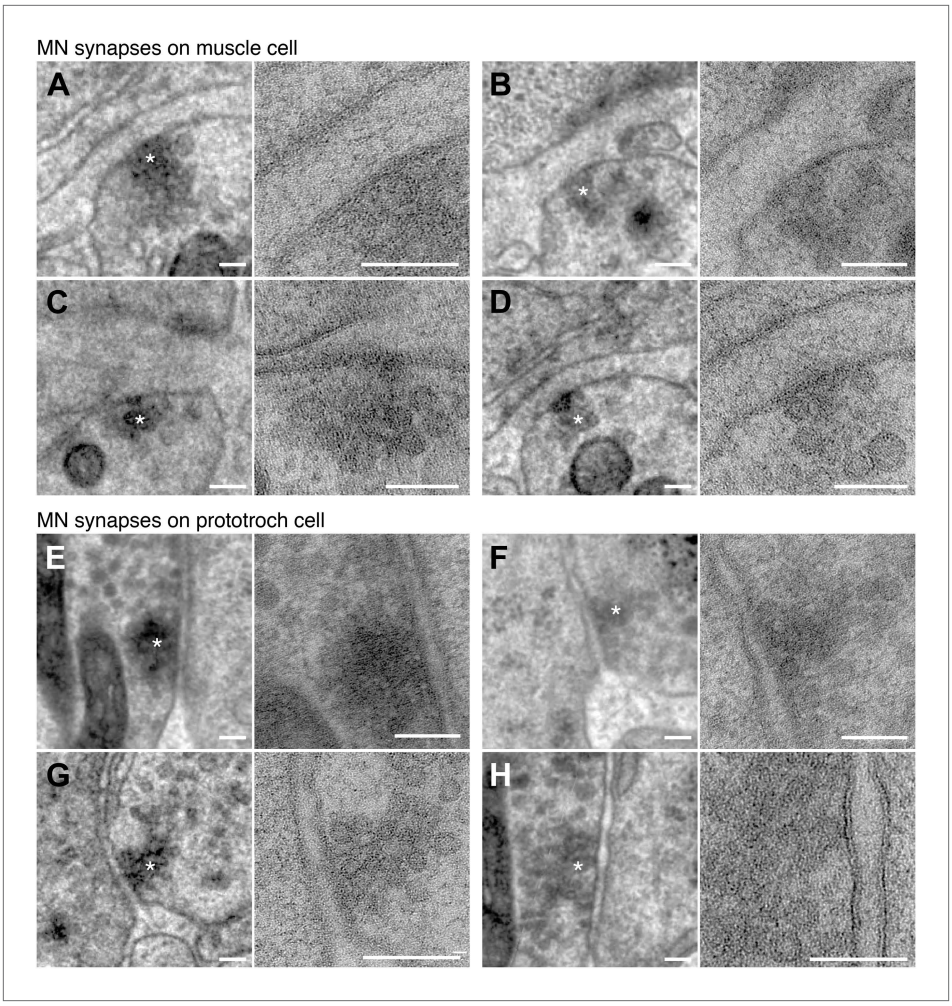

Figure 1—figure supplement 9. Synapses of motorneurons.

DOI: 10.7554/eLife.02730.012

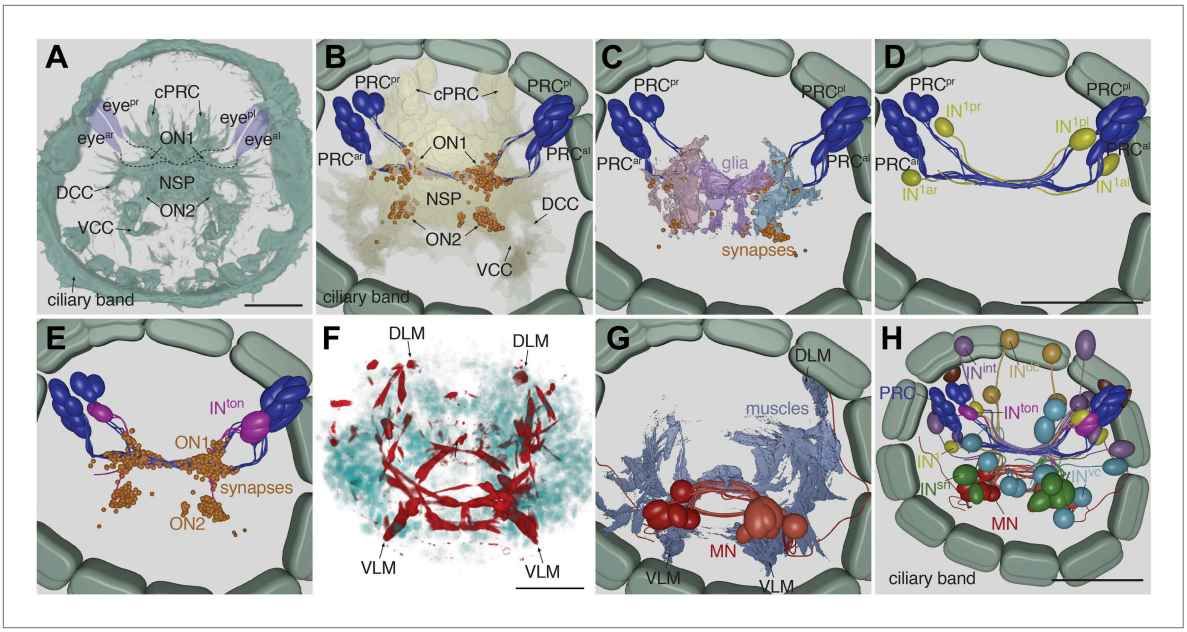

Figure 2. Cell complement of the visual circuit. (**A**) Confocal microscopic image of a 3-day-old larva stained with an anti-acetylated tubulin antibody to label neurites and cilia. Anatomical landmarks are labeled. (**B**) Blender visualization of all photoreceptor cells and all synapses of the minimal eye circuit shown in relation to the outline of neuropil, reconstructed by ssTEM. The position of synapses in the visual circuit reveals the primary and secondary optic neuropils. The schematized ciliary band cells are also shown. (**C**) ssTEM reconstruction of photoreceptors, glia cells and synapses. (**D**) ssTEM reconstruction of photoreceptors and primary interneurons (IN^{1}). (**E**) ssTEM reconstrucion showing the trans-optic-neuropil interneurons (IN^{ton}) connecting the two optic neuropils. (**F**) Confocal microscopic image of a 3-day-old larva stained with phalloidin to label the musculature (red) and with DAPI to label nuclei (cyan). (**G**) ssTEM reconstruction of muscles and motorneurons (MN). (**H**) ssTEM reconstruction of the complete cell complement of the minimal visual circuit. Neurons are colored by type. Pigment cups are shown in brown. All images show anterior views. PRC, photoreceptor; IN, interneuron; MN, motorneuron; eye^{al}, anterior-left eye; eye^{ar}, anterior-right eye; eye^{pl}, posterior-left eye; eye^{pr}, posterior-right eye; ON, optic neuropil; cPRC, ciliary photoreceptor; DCC, dorsal branch of the circumesophageal connectives; VCC, ventral branch of the circumesophageal connectives; NSP, neurosecretory plexus; DLM, dorsal longitudinal muscle; VLM, ventral longitudinal muscle. The coloring of cell types is consistent throughout the paper (PRC, blue; IN^{1}, yellow; IN^{int}, lilac; IN^{ton} , magenta; IN^{dc}, light brown; IN^{vc}, cian; IN^{sn}, green; MN, red). Scale bars, 30 μm. The Blender atlas with the volume rendering of all cells and synapses is available in ***Randel et al. (2014)***.

DOI: 10.7554/eLife.02730.016

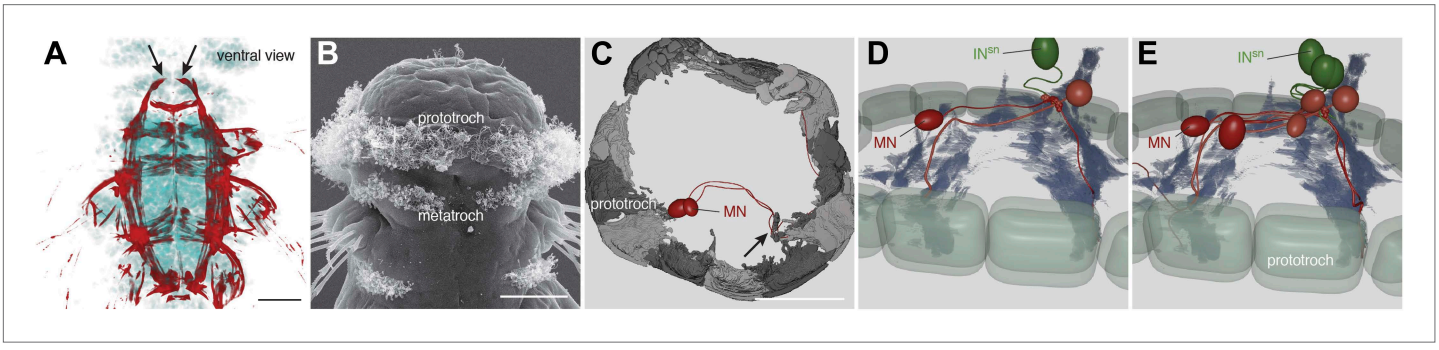

Figure 2—figure supplement 1. Muscles and ciliary bands in 3-day old larvae.

DOI: 10.7554/eLife.02730.017

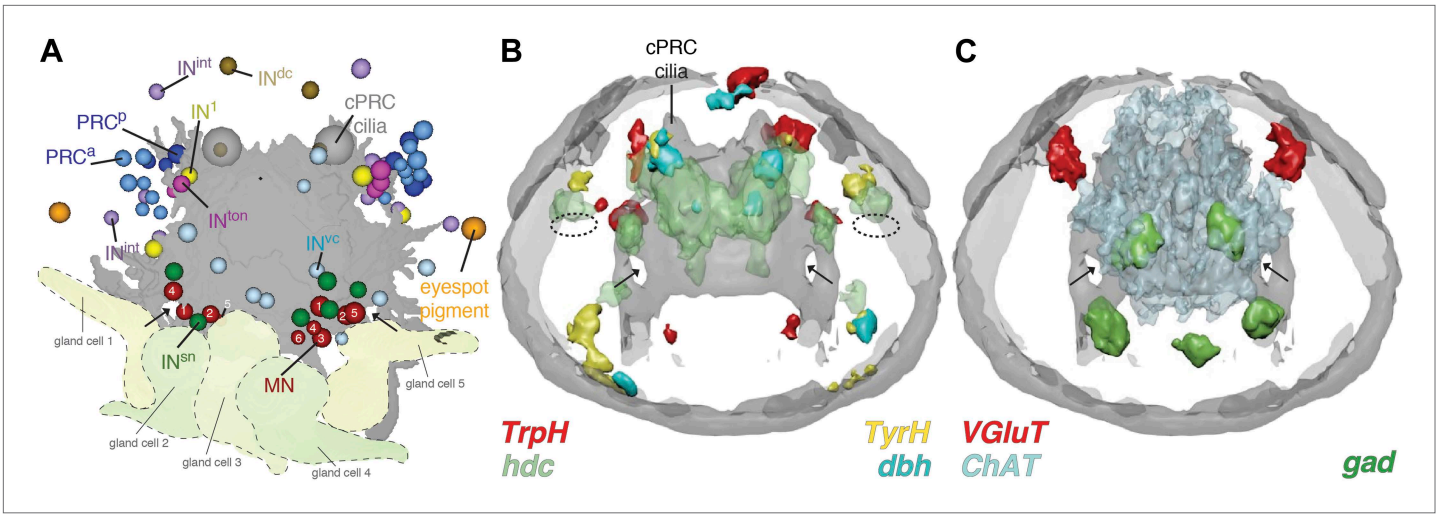

Figure 3. Neurotransmitters of the eye circuit. (**A**) Cell body positions of eye circuit neurons relative to the larval axonal scaffold and five large gland cells. Motorneurons are numbered according to the cell identifiers. (**B** and **C**) Surface representation of the average expression domains of neurotransmitter marker genes relative to the larval axonal scaffold. The following genes are shown: (**B**) histaminergic marker *histidine decarboxylase* (*hdc*; green), serotonergic marker *tryptophan hydroxylase* (*TrpH*; red), dopaminergic marker *tyrosine hydroxylase* (*TyrH*; yellow), adrenergic marker *dopamine beta hydroxylase* (*dbh*; cyan), (**C**) glutamatergic marker *vesicular glutamate transporter* (*VGluT*; red), cholinergic marker *choline acetyltransferase* (*ChAT*; grey), GABAergic marker *glutamate decarboxylase* (*gad*; green). The axonal scaffold, based on average acetylated-tubulin signal, is shown in grey. PRC, photoreceptor; cPRC, ciliary photoreceptor; IN, interneuron; MN, motorneuron. In (**B**) dashed ovals mark the position of the eyespots. Black arrows show the ring formed by the circumesophageal connectives.

DOI: 10.7554/eLife.02730.020

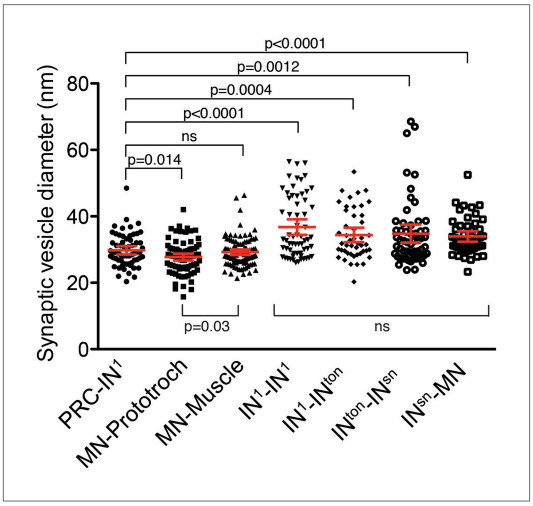

Figure 3—figure supplement 1. Synaptic vesicle diameter for different synapse types.

DOI: 10.7554/eLife.02730.021

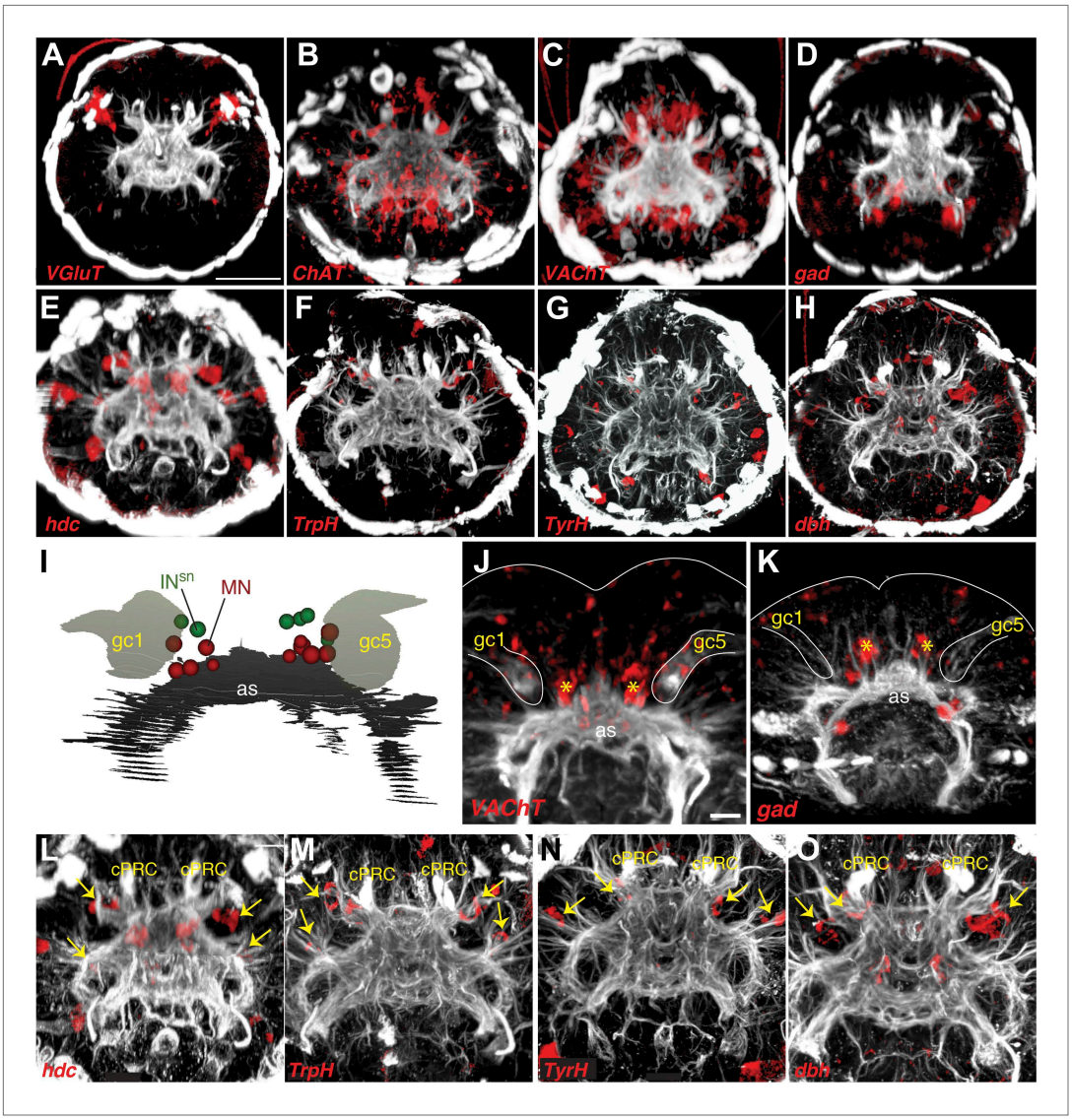

Figure 3—figure supplement 2. Expression of neurotransmitter markers in the head of *Platynereis* larva.
DOI: 10.7554/eLife.02730.022

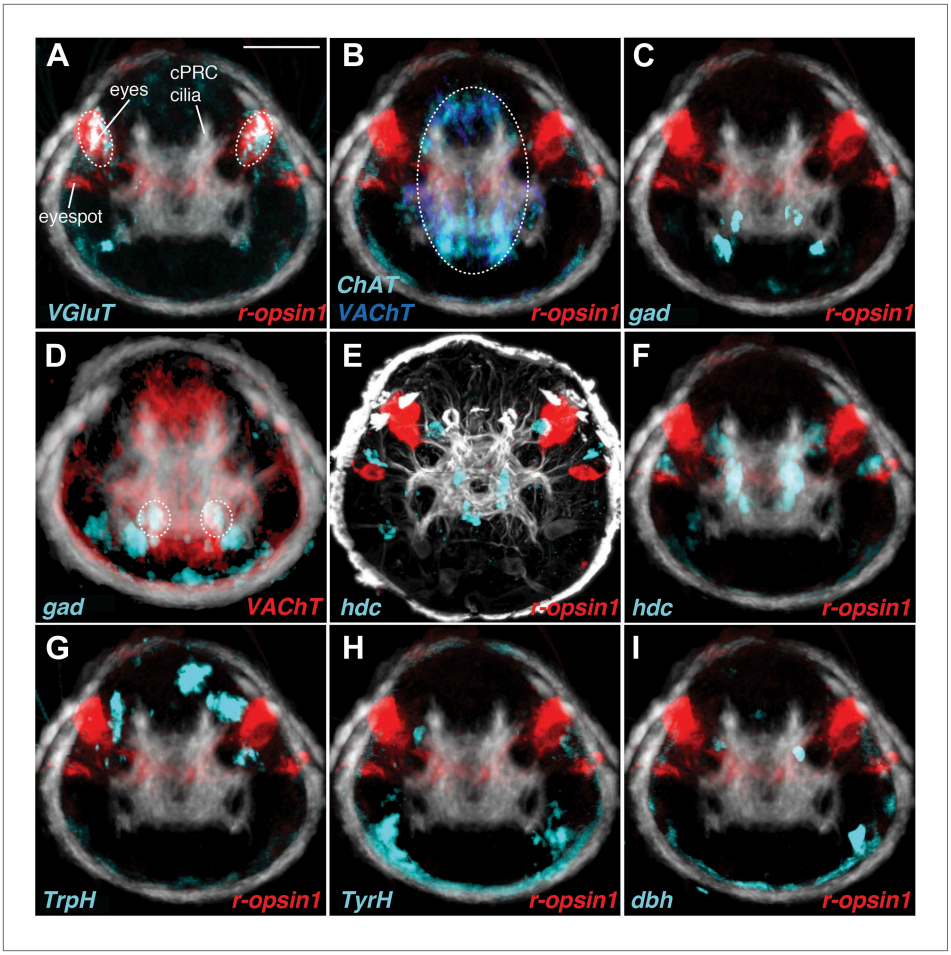

Figure 3—figure supplement 3. Neurotransmitter marker gene expression profiling.

DOI: 10.7554/eLife.02730.023

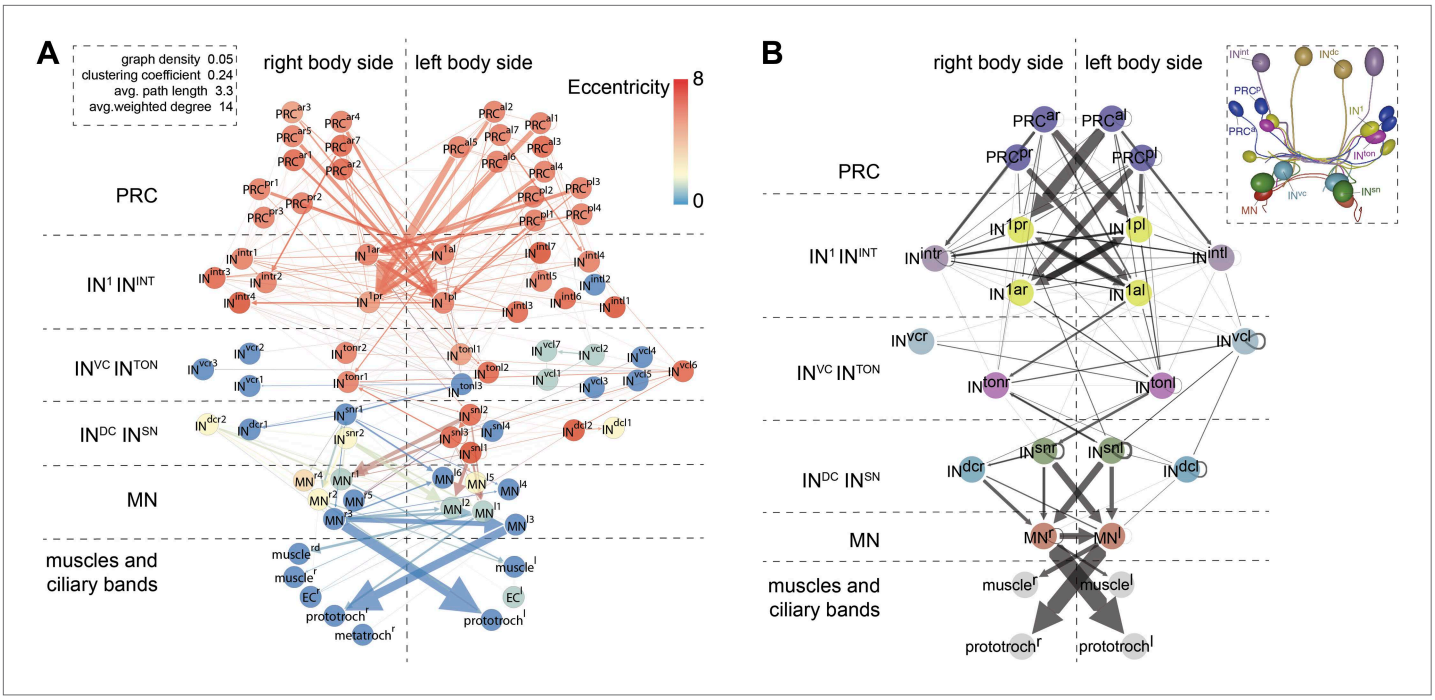

Figure 4. Network analysis of the visual eye circuitry. (**A**) Full connectomic graph of the visual eye circuit including 71 neurons and 8 effectors (muscles, ciliary band cells and epithelial cells). The edges are directed from presynaptic cell pointing to postsynaptic cells. Edges are weighted by the number of synapses. Inset shows selected network parameters. (**B**) Merged graph representation of the visual circuit. Nodes correspond to neuron classes, edges are weighted by the maximum number of synapses between two neuron types of each class. Nodes are colored following the color scheme used to label cell types. Inset shows the anatomical position of the cell types. PRC^{al}, anterior-left photoreceptors; PRC^{ar}, anterior-right photoreceptors; PRC^{pl}, posterior-left photoreceptors; PRC^{pr}, posterior-right photoreceptors; IN, interneuron; MN, motorneuron. Matrix files of the complete and the merged networks are available in ***Figure 4—source datas 1 and 2***.

DOI: 10.7554/eLife.02730.024

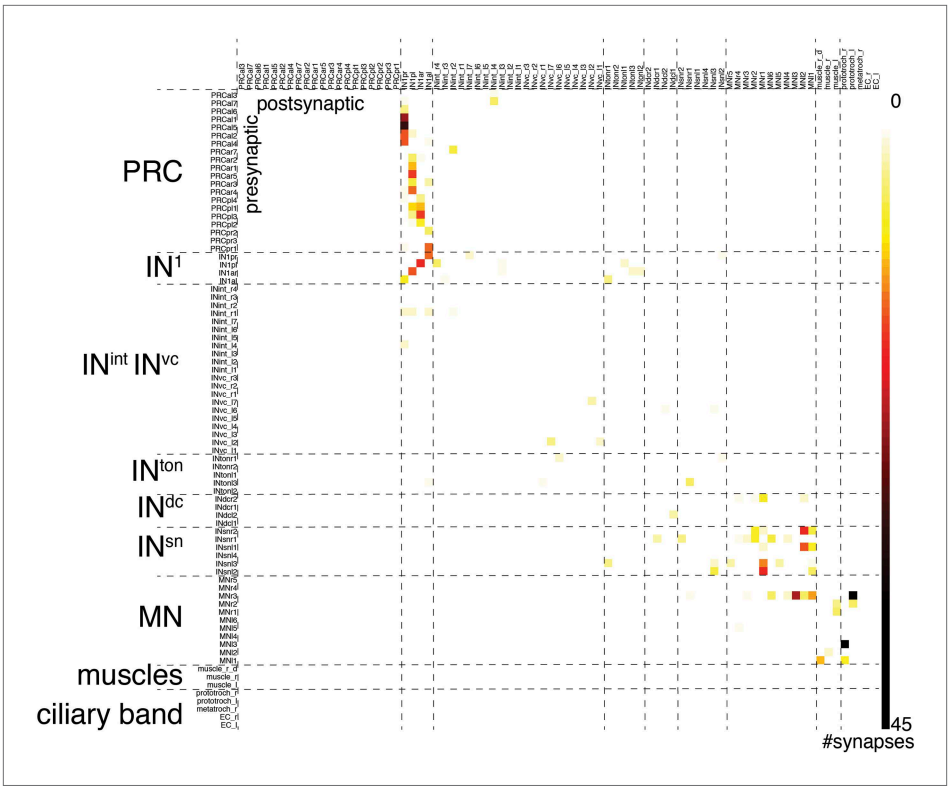

Figure 4—figure supplement 1. Synaptic connectivity matrix of the *Platynereis* larval visual circuit.
DOI: 10.7554/eLife.02730.027

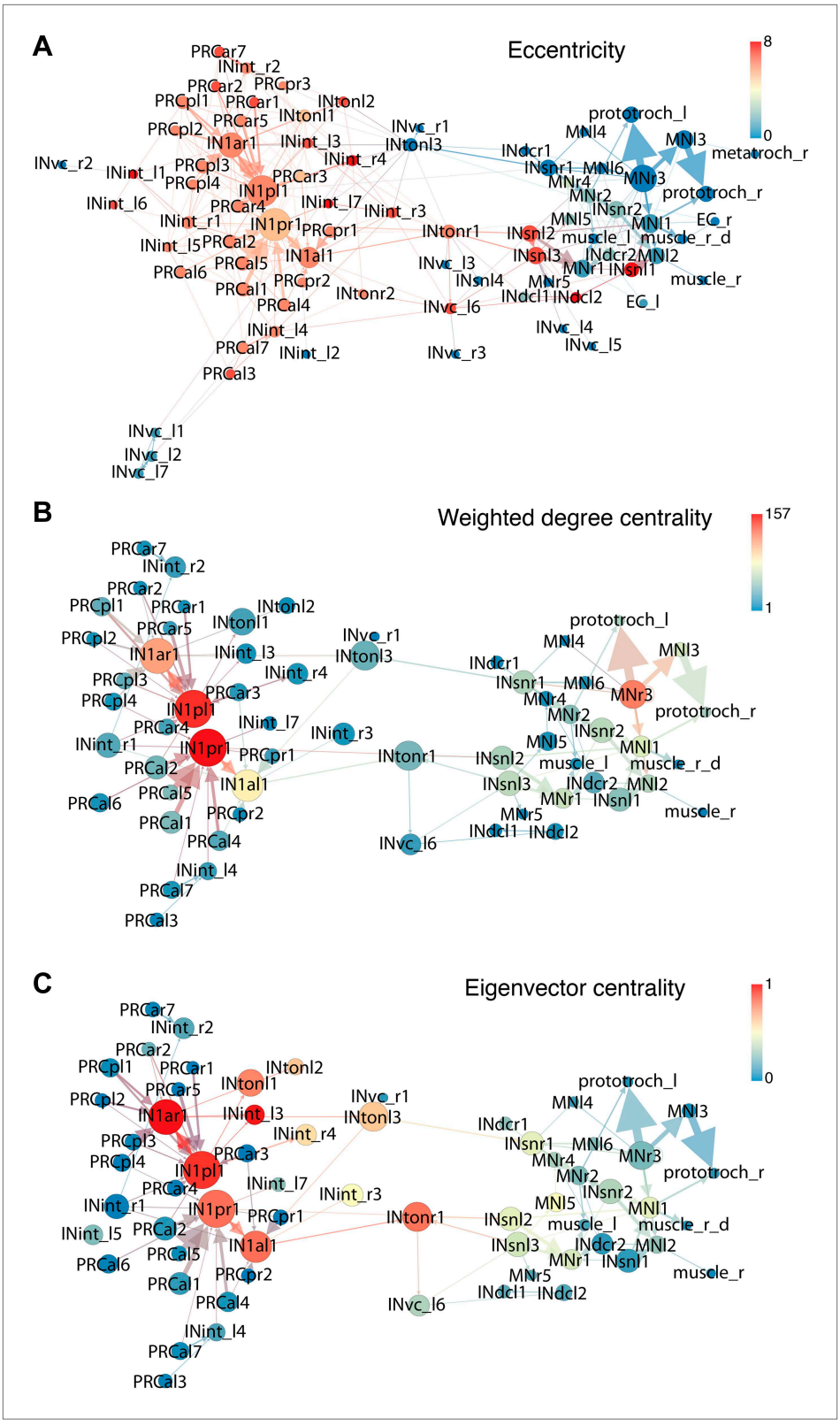

Figure 4—figure supplement 2. Connectivity graphs of the *Platynereis* larval visual circuit.

DOI: 10.7554/eLife.02730.028

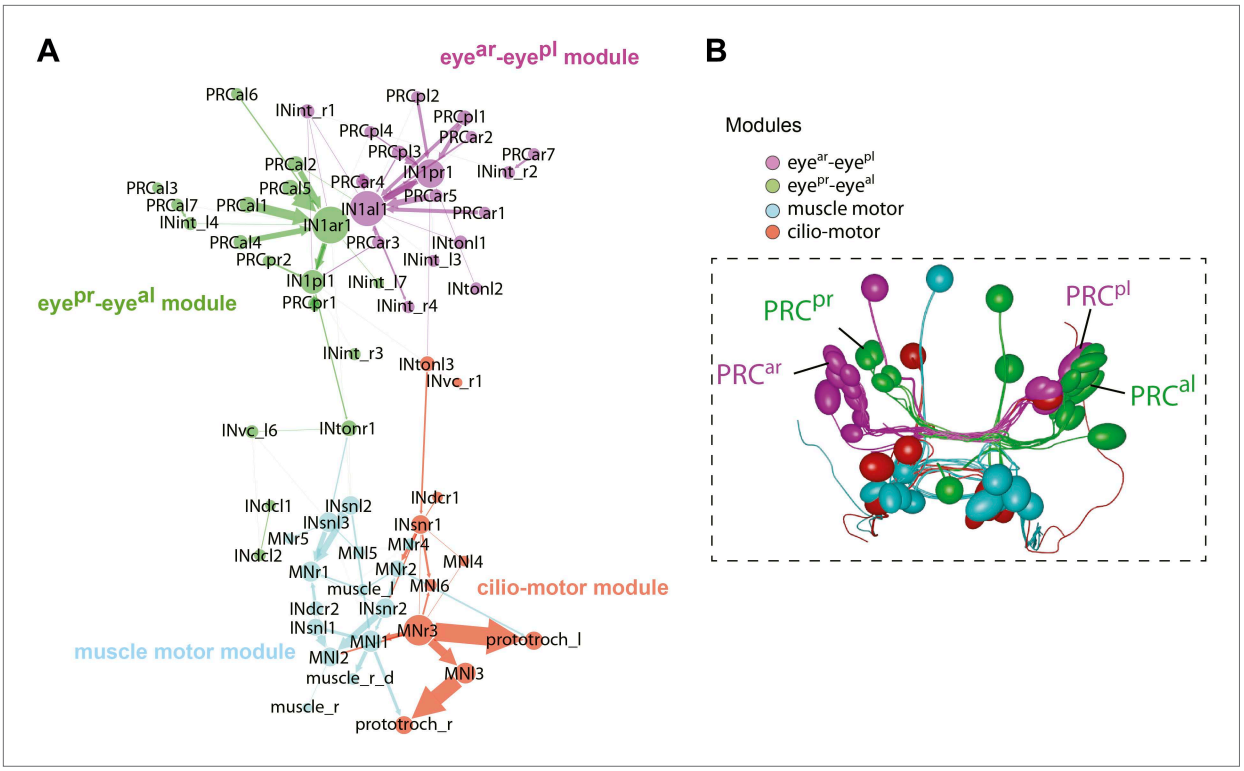

Figure 4—figure supplement 3. Modules in the eye connectivity graph.

DOI: 10.7554/eLife.02730.029

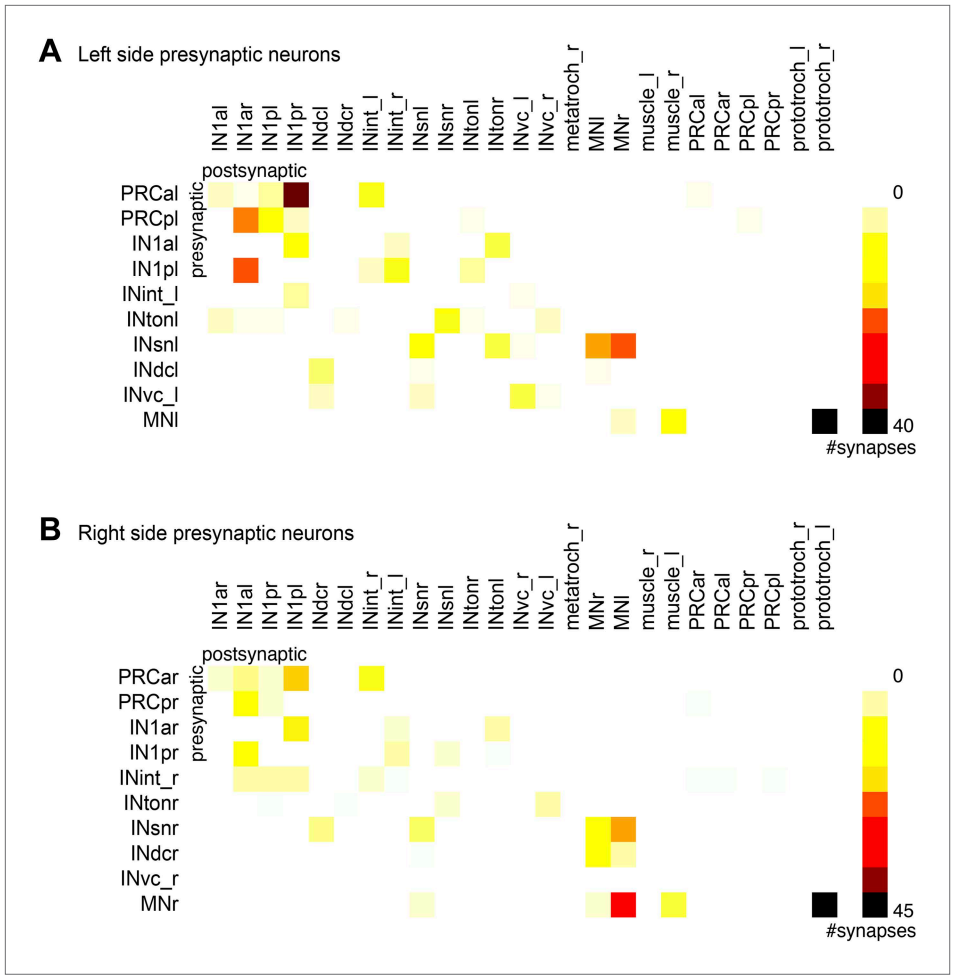

Figure 4—figure supplement 4. Connectivity matrix of the left and right body sides.

DOI: 10.7554/eLife.02730.030

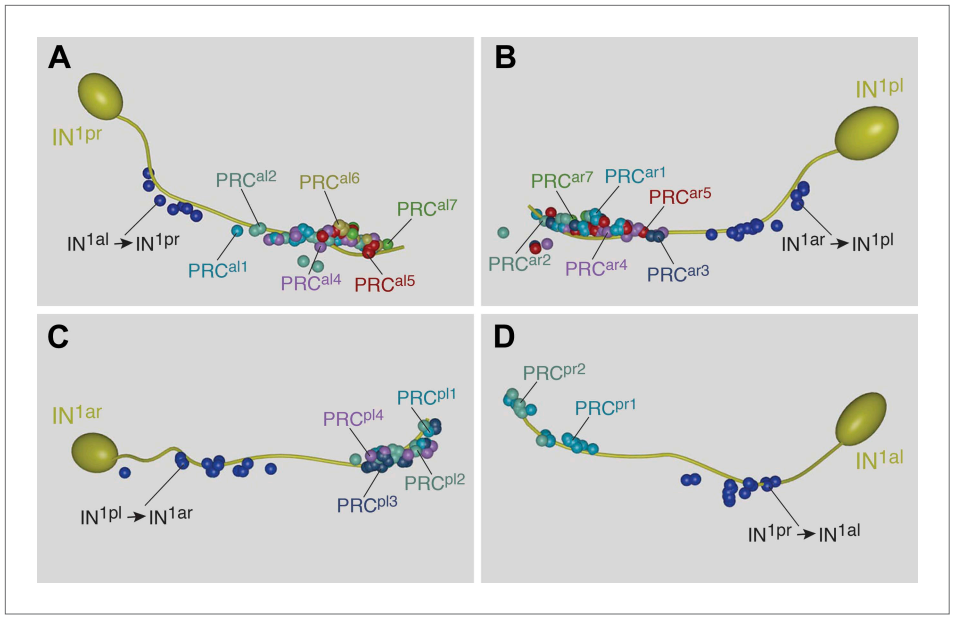

Figure 4—figure supplement 5. Stereotypy of synapse distribution on IN[1] cells.

DOI: 10.7554/eLife.02730.031

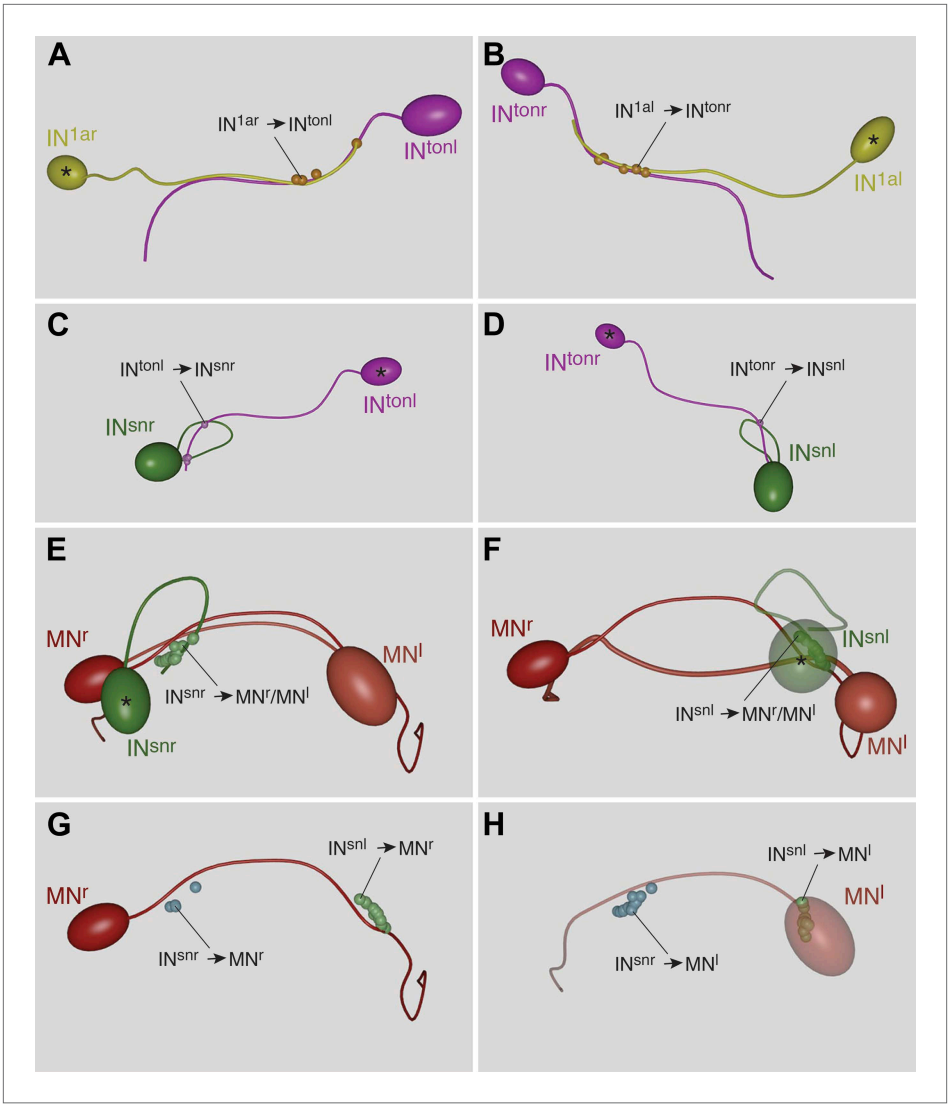

Figure 4—figure supplement 6. Stereotypy of synapse distribution on IN^{ton}, IN^{sn} and MN cells.
DOI: 10.7554/eLife.02730.032

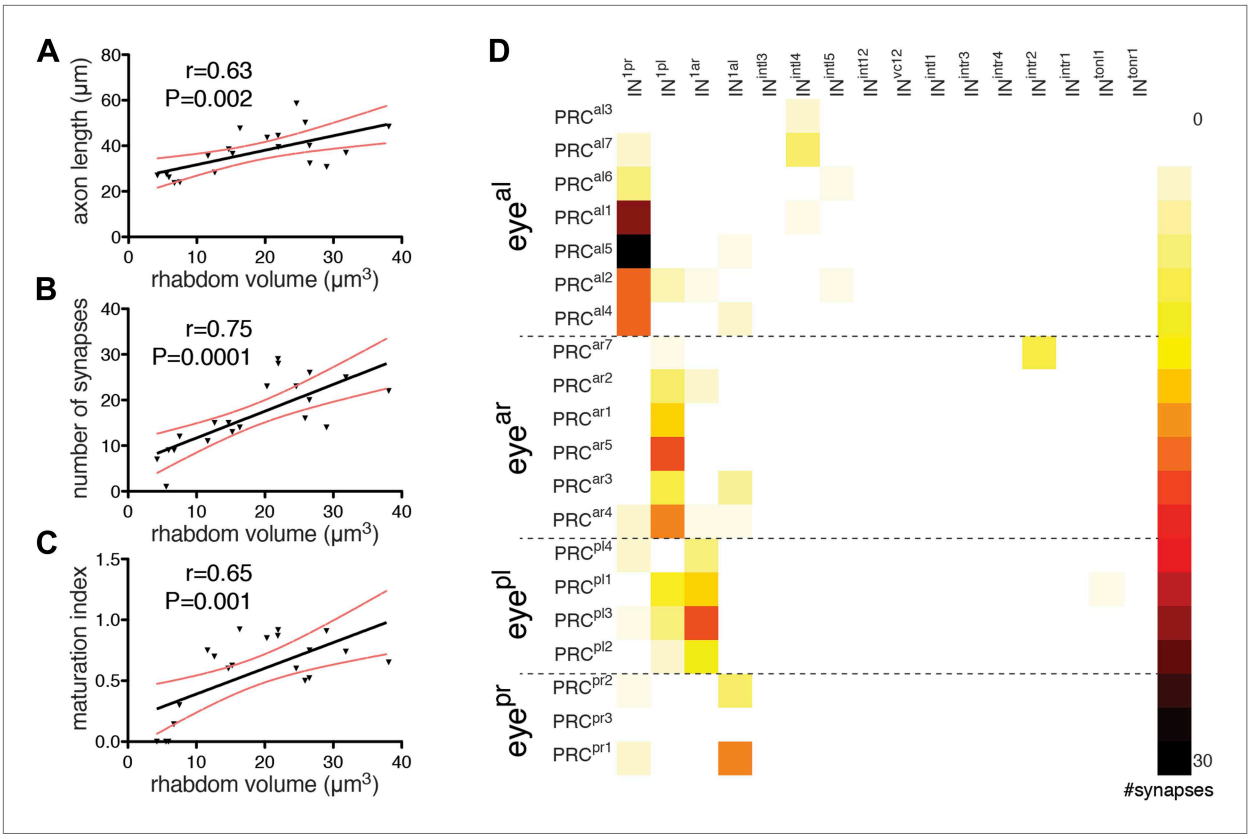

Figure 5. Maturation of photoreceptor connections. (**A**) Relationship of rhabdom volume to photoreceptor axon length. (**B**) Relationship of rhabdom volume to photoreceptor synapse number. (**C**) Relationship of photoreceptor connectivity-maturation index to rhabdom volume. In **A**–**C** the black line shows linear regression with 95% confidence interval (red dashed lines). Pearson r and p-value are shown. (**D**) Connectivity matrix of the photoreceptors. The matrix is ordered from top to bottom by eye and then for each eye by photoreceptor rhabdom size increasing from top to bottom. Eye^{al}, anterior-left eye; eye^{ar}, anterior-right eye; eye^{pl}, posterior-left eye; eye^{pr}, posterior-right eye.

DOI: 10.7554/eLife.02730.033

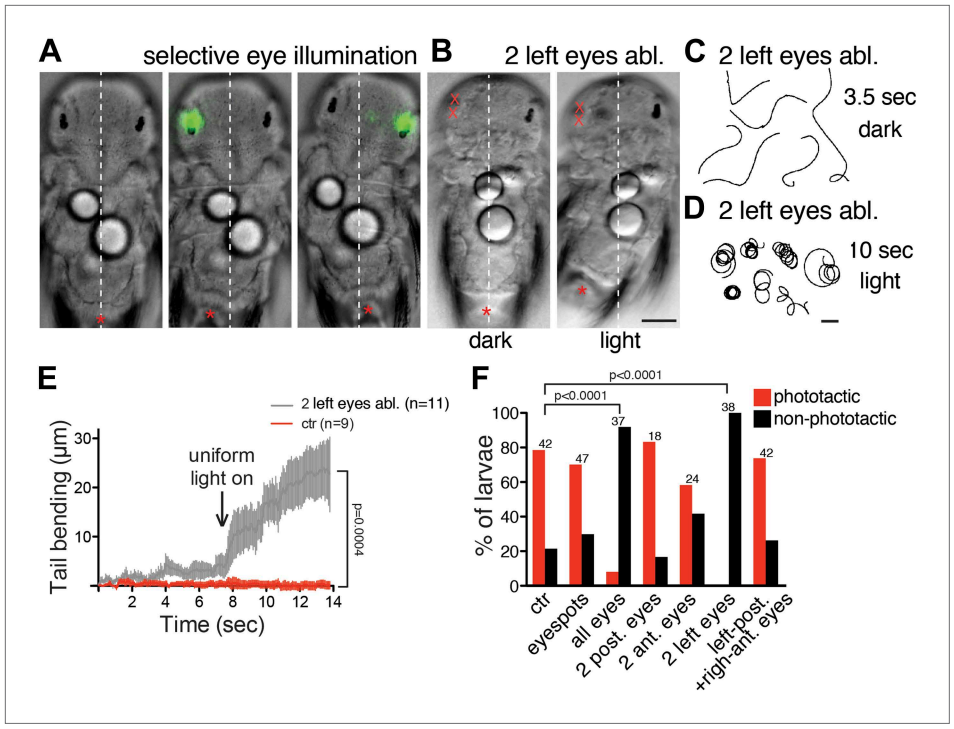

Figure 6. Eyes mediate body bending during visual phototaxis. (**A**) Selective eye illumination triggers body bending in an immobilized larva. (**B**) A larva with both left eyes ablated displays body bending upon uniform illumination with white light (light) but not with a red filter (dark). An asterisk marks the tip of the tail. (**C** and **D**) Trajectories of larvae with both left eyes ablated in the dark (red filter) (**C**) and upon uniform illumination with white light (**D**). (**E**) Tail bending upon uniform white light illumination of non-ablated control larvae and larvae lacking the two left eyes. Data are shown as mean ± SEM, n >9 for both condition. p-value of a *t* test calculated for the last time point is indicated. (**F**) Percentage of phototactic (red) and non-phototactic (black) larvae among non-ablated control and various eye-ablated larvae. p-values of a chi-square test are indicated relative to non-ablated controls. Only the 'all eyes' and 'two left eyes' ablated conditions are significantly different from non-ablated control. Number of larvae tested is shown above the columns for each condition. Scale bars, 40 µm (**A** and **B**), 1 mm (**C** and **D**).

DOI: 10.7554/eLife.02730.036

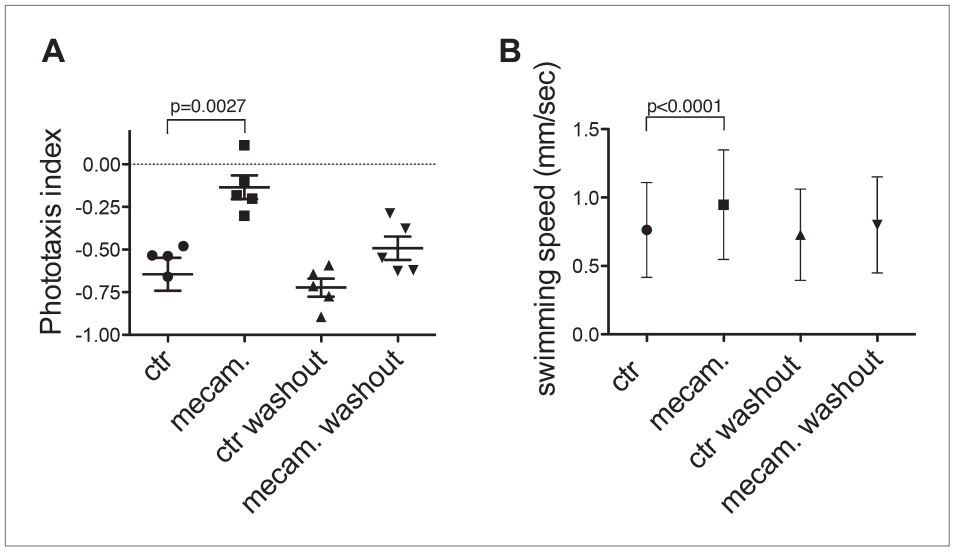

Figure 6—figure supplement 1. Inhibition of phototaxis by a cholinergic antagonist.

DOI: 10.7554/eLife.02730.037

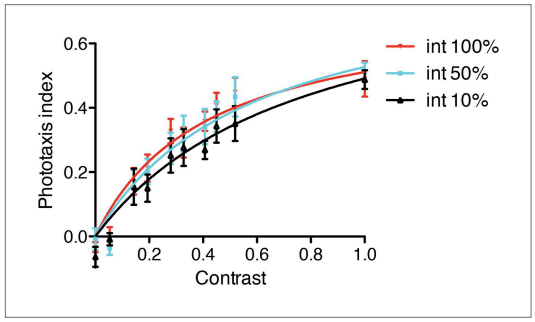

Figure 6—figure supplement 2. Efficiency of phototaxis depends on contrast, not absolute light levels.

DOI: 10.7554/eLife.02730.038

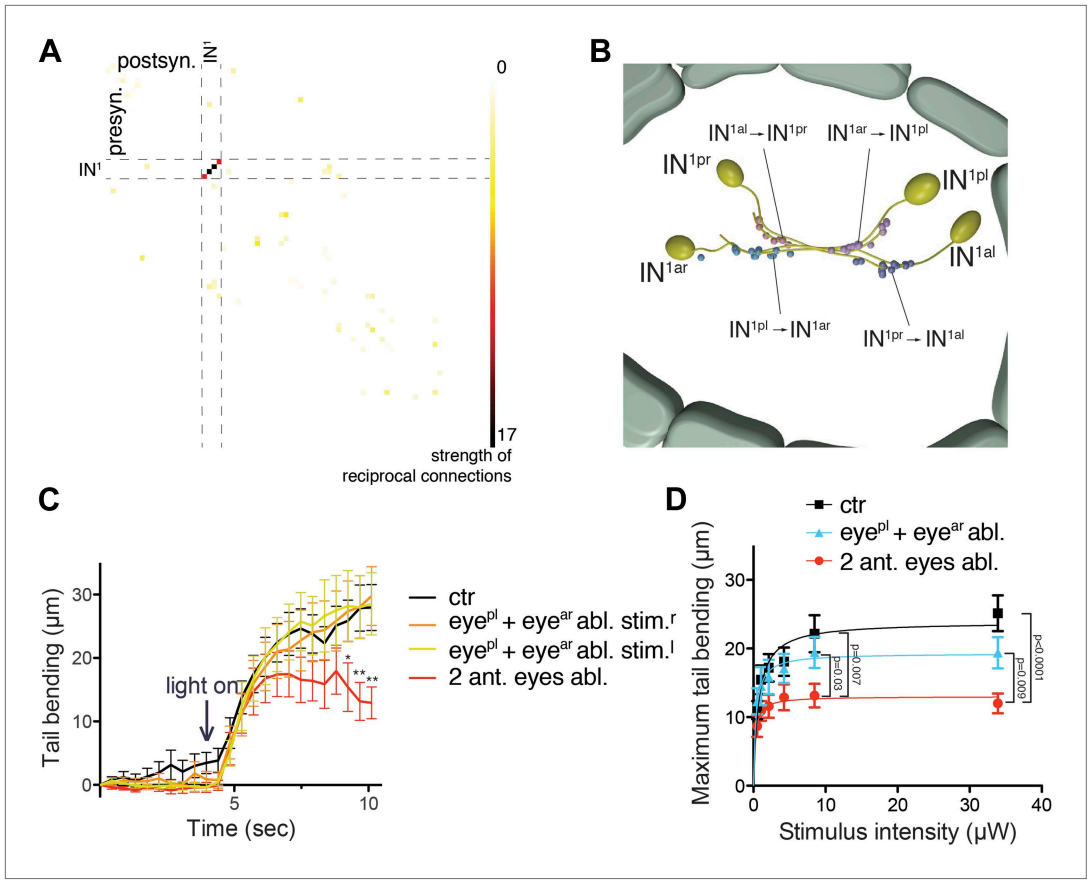

Figure 7. An interneuron motif for enhanced contrast detection. (**A**) Strength of reciprocal connections between all neuron pairs in the complete visual circuit. The strength of reciprocal connections was defined as the geometric mean of the number of reciprocal synapses between each neuron pair. The single neuron identifiers are not shown for simplicity. (**B**) The strongest reciprocal motif in the eye circuit is between the crosswise IN^{1} pairs. The position and polarity of the synapses are indicated. (**C**) Quantification of tail bending in different eye ablated larvae under selective eye illumination with a 488-nm laser. Data are shown as mean ± SEM, n >17 for each condition. Larvae lacking two anterior eyes were compared to non-ablated control larvae at each time point (*p value<0.05, **p value<0.01, unpaired *t* test). (**D**) Signal-response curve of maximum tail bending upon selective eye illumination in immobilized larvae using 488-nm stimuli of different intensities. The data are fitted with a saturation-binding curve. Data are shown as mean ± SEM, n >24 larvae for each condition (independent from **C**). p-values of unpaired *t* tests comparing larvae lacking two anterior eyes to the other conditions are shown. Source bending data from (**C** and **D**) are shown in ***Figure 7—source data 1*** and ***Figure 7—source data 2***.

DOI: 10.7554/eLife.02730.040

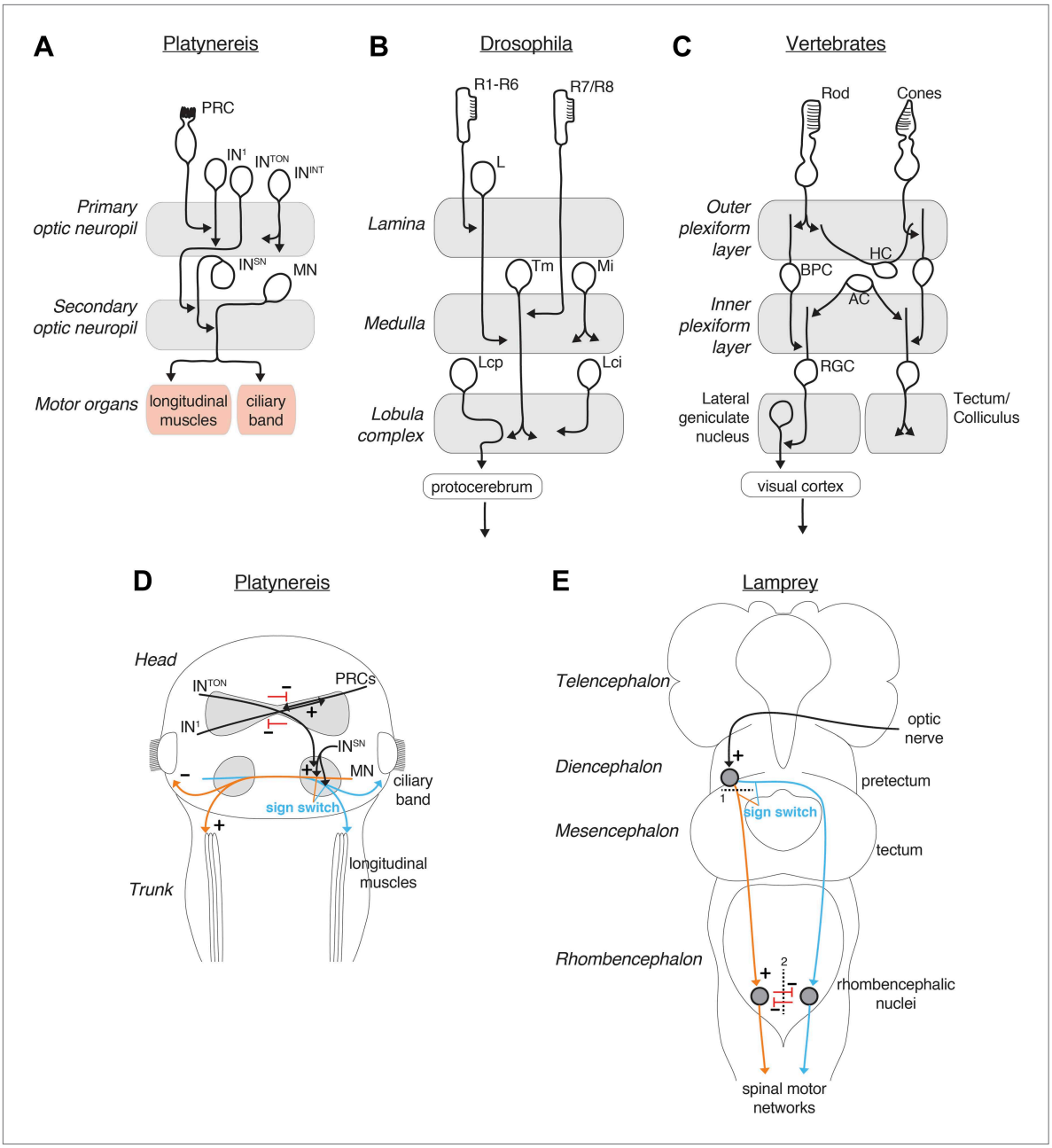

Figure 8. Comparison of the *Platynereis, Drosophila* and vertebrate visual circuits. Comparison of the *Platynereis* visual circuit with the *Drosophila* and vertebrate visual circuits on the neuronal level (**A**–**C**) and with the lamprey phototactic circuit on the circuit level (**D** and **E**). In (**E**) dashed line (1) represents a mesencephalic hemisection, severing connections between the pretectum and the ipsilateral reticulospinal neurons, dashed line (2) represents transection of the ventral rhombencephalic commissure. L, lamina monopolar neuron; Tm, transmedula neuron; Mi, medulla intrinsic neuron; Lcp, lobula complex projection neuron; Lci, lobula complex intrinsic neuron; BPC, bipolar cell; HC, horizontal cell, AC, amacrine cell; RGC, retinal ganglion cell. (**B** and **C**) after ***Erclik et al. (2009)***; (***Sanes and Zipursky, 2010***) (**E**) after ***Ullén et al. (1997)***.

DOI: 10.7554/eLife.02730.047